Sb2S3/TiO2 Heterojunction Photocathodes: Band Alignment and Water Splitting Properties

Prabhakar, Rajiv Ramanujam ; Moehl, Thomas ; Siol, Sebastian ; Suh, Jihye ; Tilley, David

Abstract: Antimony sulfide (Sb2S3) is a promising light-absorbing semiconductor for photovoltaic applications, though it remains vastly unexplored for photoelectrochemical water splitting. Sb2S3 was synthesized by a simple sulfurization of electrodeposited antimony metal at relatively low temperatures (240–300 °C) with elemental sulfur. Using a TiO2 buffer layer and a platinum co-catalyst, photocurrent densities up to 9 mA cm–2 were achieved at −0.4 V vs RHE in 1 M H2SO4 under one sun illumination. Using X-ray photoelectron spectroscopy band alignment studies and potential-dependent incident photon-to-current efficiency measurements, a conduction band offset of 0.7 eV was obtained for the Sb2S3/TiO2 junction as well as an unfavorable band bending at the heterointerface, which explains the low photovoltage that was observed (0.1 V). Upon inserting an In2S3 buffer layer, which offers a better band alignment, a 0.15 V increase in photovoltage was obtained. The excellent photoelectrochemical water splitting performance and the identification of the origin of the low photovoltage of the Sb2S3 photocathodes in this work pave the way for the further development of this promising earth-abundant light-absorbing semiconductor for solar fuel generation.

DOI: https://doi.org/10.1021/acs.chemmater.0c01581

Sb_2S_3/TiO_2 Heterojunction Photocathodes: Band Alignment and Water Splitting Properties

Rajiv Ramanujam Prabhakar, Thomas Moehl, Sebastian Siol, Jihye Suh, and

S. David Tilley*

ABSTRACT

Antimony sulfide (Sb_2S_3) is a promising light absorbing semiconductor for photovoltaic applications, though it remains vastly unexplored for photoelectrochemical water splitting. Sb_2S_3 was synthesized by a simple sulfurization of electrodeposited antimony metal at relatively low temperatures (240-300°C) with elemental sulfur. Using a TiO_2 buffer layer and a platinum co-catalyst, photocurrent densities up to ~ 9 mA cm^{-2} were achieved at -0.4 V vs. RHE in 1 M H_2SO_4 under one sun illumination. Using XPS band alignment studies and potential dependent IPCE measurements, a conduction band offset of 0.7 eV was obtained for the Sb_2S_3/TiO_2 junction as well as an unfavorable band bending at the heterointerface, which explains the low photovoltage that was observed (~ 0.1 V). Upon inserting an In_2S_3 buffer layer, which offers a better band alignment, a 0.15 V increase in photovoltage was obtained. The excellent PEC performance and the identification of the origin of the low photovoltage of the Sb_2S_3 photocathodes in this work pave the way for the further development of this promising earth abundant light absorbing semiconductor for solar fuels generation.

TOC Graphic

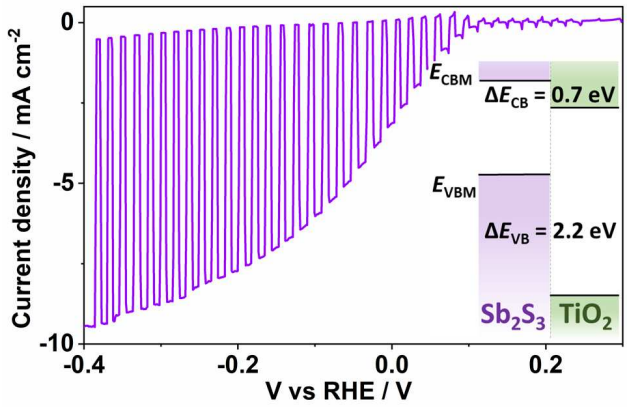

INTRODUCTION

Antimony sulfide (Sb_2S_3) has attracted interest in the photovoltaic (PV) community, primarily in solid state sensitized solar cells though more recently with thin film solar cells.[1] Sb_2S_3 is composed of earth abundant relatively non-toxic constituents with a band gap of 1.7 eV and a high absorption coefficient.[2] In PV research, Sb_2S_3 has been explored in both semiconductor-sensitized and thin film solar cell architectures, where the Sb_2S_3 was mostly synthesized by chemical bath deposition (CBD), yielding efficiencies of greater than 7%.[3–5] Despite the broad interest and promising efficiency in PV research, Sb_2S_3 has not yet been explored extensively for photoelectrochemical water splitting (PEC) applications. Sb_2S_3 has been employed as a heterojunction partner for WO_3 and TiO_2 photoanodes for water splitting.[6,7] DeAngelis et al. reported an Sb_2S_3 photoanode for water splitting yielding photocurrent densities exceeding 4 mA cm^{-2}, however, very low faradaic efficiencies for oxygen evolution were observed, and hence the current obtained was primarily due to photocorrosion.[8] Very recently, Wang et al reported an Sb_2S_3 photocathode using a toxic CdS buffer layer.[9] However, an in depth investigation on the Sb_2S_3/buffer layer junction properties and identification of photovoltage loss mechanisms in the Sb_2S_3 photocathode is lacking.

In this work, we report a Sb_2S_3 photocathode using TiO_2 and In_2S_3 as buffer layers for PEC water splitting. Sb_2S_3 thin films were fabricated using a simple, relatively low temperature sulfurization (240°C-300°C) of Sb metal. Sb_2S_3 thin films were obtained and photocathodes were fabricated using TiO_2 as a buffer layer/protection layer, which yielded high photocurrents of ~ 3 mA cm^{-2} at 0 V vs. RHE in 1 M H_2SO_4 when coated with platinum (Pt) as the hydrogen evolution reaction (HER) catalyst. Using X-ray photoelectron spectroscopy (XPS), the band alignment of the Sb_2S_3/TiO_2 junction was investigated and a conduction band offset (CBO) of 0.7 eV was found.

The measured CBO partly explains the low photovoltage in the Sb_2S_3/TiO_2 junction, and we sought to mitigate this by using a buffer layer with a higher lying conduction band, which should lessen the CBO. A higher photovoltage was indeed obtained using In_2S_3 as buffer layer (0.15 V increase), which has a higher conduction band maximum than TiO_2. To the best of our knowledge, Sb_2S_3/In_2S_3 photocathodes investigated here have not yet been reported for photoelectrochemical water splitting.

EXPERIMENTAL SECTION

Synthesis of Sb_2S_3 thin films: Synthesis of Sb_2S_3 was carried out by electrodeposition of Sb metal on Au-coated (150 nm) fluorine doped tin oxide (FTO) substrates, followed by annealing in sulfur atmosphere. The experimental procedure for electrodeposition of Sb metal has been previously reported.[10] Briefly, Sb metal was electrodeposited on Au-coated FTO substrates in a three-electrode configuration using a solution of potassium antimonyl tartrate ($K_2(Sb_2(C_4H_2O_6)_2)$ and tartaric acid at a pH of 1.3 (adjusted using sulfuric acid) and a potential of -0.3 V vs Ag/AgCl. The Sb metal was then annealed in sulfur atmosphere at different temperatures, ranging from 240 to 300 °C. The sulfurization process was carried out in a 2-zone furnace (**Figure S1**). The tube furnace was evacuated using a vacuum pump and then filled with Ar. This process was repeated 3 times and the sulfurization was carried out under a base pressure of Ar (0.5 bar). A ramping rate of ~ 12°C/min was used to reach the desired sulfurization temperature. The Sb metal on Au-coated FTO substrates were placed in zone 1 (240-300 °C) and elemental sulfur powder (500 mg) was placed in zone 2 (200 °C). The sulfurization was carried out for 40 minutes followed by cooling naturally to room temperature over 60 minutes.

Raman spectroscopy: Raman spectra were obtained using a Renishaw System (excitation wavelength 532 nm and laser spot size ~2 μm).

X-Ray diffraction: The crystal structure of Sb_2S_3 electrodes were examined by X-ray diffraction using a Rigaku SmartLab instrument (Cu K_α radiation) at 2 deg min^{-1} with a step width of 0.01 deg in 2θ-ω scan mode.

Atomic Force Microscopy and Kelvin Probe Measurements: An Asylum Research AFM (MFP-3D) was used to measure the surface morphology and the contact potential difference (CPD) in tapping mode. The probe used for the measurement was an AC240TM-R3 from Olympus. The open source Gwyddion software package as well as the Asylum Research built in software were used to further analyze the AFM pictures. The AFM cantilevers were calibrated against highly oriented pyrolytic graphite (HOPG) to relate the CPD to the actual work function of the investigated samples. As high-resolution topographic AFM measurements in combination with CPD measurements took several hours and the tip reference potential can change during such measurement, fast (5-10 min) CPD measurement of the samples were performed first (variation of the CPD was below 50 mV between the different samples) and used as calibration for the work function of the long topography and CPD measurements (with higher resolution).

***Atomic Layer Deposition of TiO_2*:** TiO_2 was deposited by atomic layer deposition (ALD) using a Picosun R200 tool. The reactor temperature for deposition was 120 °C and the titanium precursor was tetrakis(dimethylamino)titanium (TDMAT) (precursor temperature 85°C), with water used as the oxygen source. The thickness of the ALD TiO_2 was ~ 100 nm, as measured by ellipsometry on a silicon witness wafer.

Chemical bath deposition of In_2S_3: In_2S_3 was deposited by chemical bath deposition on the Sb_2S_3 thin films using a solution of 0.971 g of $In_2(SO_4)_3$ (25 mM), 0.563 g of CH_3CSNH_2 (0.1 M) and 0.43 ml CH_3COOH (0.1 M) in 75 ml de-ionized water.[11] All the chemicals were first dissolved in 75 ml de-ionized water in a beaker and then placed in a bath pre-heated to 70°C. After about 45 mins, a faint yellow precipitate was formed, which is the indication that In_2S_3 has started to precipitate, and then the Sb_2S_3 thin films were immersed for a duration of 15 mins. Next, the films were thoroughly rinsed with de-ionized water and dried under a stream of nitrogen.

***Photoelectrodeposition of platinum catalyst*:** Platinum catalyst was photoelectrodeposited from an aqueous solution of 1 M Na_2SO_4 containing 1 mM H_2PtCl_6, using a constant current of -0.05 mA cm^{-2} for 10 min under 1 sun illumination.

***Photoelectrochemical characterization of Sb_2S_3 photocathodes*:**

The photoelectrochemical performance of the photocathodes was evaluated in a three-electrode configuration using a BioLogic SP-200 potentiostat under irradiation from simulated AM 1.5 G illumination, calibrated using a silicon diode from PV Measurements, Inc. (100 mW cm^{-2}). A 1 M H_2SO_4 (pH 0) solution was used as the electrolyte. The reference electrode was Ag /AgCl (sat'd KCl), and a Pt wire was used as the counter electrode. Before measurement, the electrolyte was sparged with N_2 for at least 30 min to remove dissolved oxygen. The photocathode area was defined using epoxy (Loctite 9461) and the active area was determined by counting pixels using the image processing software gimp. The onset potential was estimated by extrapolating the steep rise of the photocurrent in the current density-voltage plots to the voltage axis and the corresponding intercept

was used as the onset potential. The conversion between potentials vs. Ag/AgCl and vs. RHE was performed using the equation:

$$E\ (\text{vs. RHE}) = E\ (\text{vs Ag/AgCl}) + 0.059\ \text{V} \times \text{pH} + 0.197\ \text{V}\ (E_{Ag/AgCl})$$

Incident photon-to-current efficiency (IPCE) was measured on a home-built IPCE system featuring a halogen light source with double monochromator and white light bias. The IPCE was measured in a three-electrode configuration using Ag/AgCl (sat'd KCl) reference electrode and Pt wire as the counter electrode at 0 V versus RHE in 1 M H_2SO_4 (pH 0) at 5 nm wavelength intervals. To compare the wavelength dependent change of the IPCE at different bias potentials, the IPCE values from the measurement at 0.05 V vs RHE was normalized (multiplied) to reach the same value at 540 nm as for the measurements at more negative applied potentials.

X-ray photoelectron spectroscopy (XPS): XPS was conducted using a Physical Electronics (PHI) Quantum 2000 X-ray photoelectron spectrometer featuring monochromatic Al Kα radiation, generated from an electron beam operated at 15 kV and 32.3 W. The energy scale of the instrument was calibrated using Au and Cu reference samples. The analysis was conducted at 1×10^{-6} Pa, with an electron take off angle of 45° and a pass energy of 23.50 eV. Core level binding energies were determined fitting Voigt profiles (GL30) after Shirley background subtraction. No charge neutralization was used throughout the measurement. The neutralizer was toggled to ensure the samples were sufficiently conductive. The main component of the C 1s emission for the Sb_2S_3 substrate was found to be at 284.72 eV. The valence band offset was determined using a procedure based on the Kraut method,[12] which is described in more detail by Klein and coworkers.[13]

RESULTS AND DISCUSSION

Synthesis, morphology and crystallinity of Sb_2S_3 thin films:

Synthesis of Sb_2S_3 was carried out by electrodeposition of Sb metal on Au-coated fluorine doped tin oxide (FTO) substrates, followed by annealing in excess sulfur atmosphere. An excess of sulfur was employed in order to maintain a sulfur rich atmosphere during the conversion of Sb metal to Sb_2S_3. X-ray diffraction (XRD) patterns were obtained to evaluate the crystallinity of the Sb_2S_3 films at different sulfurization temperatures (**Figure 1 (a-c)**). All diffractions were indexed to the orthorhombic phase (JCPDS 00-006-0474) of Sb_2S_3, though the most intense peaks derived from the substrate. $AuSb_2$ peaks were observed at all sulfurization temperatures indicating alloying of Sb with the Au back contact. Raman spectra of the samples were obtained at the different sulfurization temperatures to further confirm whether Sb_2S_3 was formed (**Figure S2**). All films exhibited two strong peaks, one at 285 cm^{-1} and the other at 305 cm^{-1}, which are characteristic of Sb-S stretching modes (A_g modes), confirming that the films were phase pure Sb_2S_3.[14]

The surface morphology of the synthesized films was investigated by scanning electron microscopy (SEM). No discernable differences were observed in the morphology of the Sb_2S_3 films for 240°C and 270°C sulfurization temperatures (**Figure 1 (d) and (e)**). In contrast, long triangular rod-like grains were observed for the samples sulfurized at 300°C (**Figure 1 (f) and Figure S3**). Characterization by atomic force microscopy (AFM) confirmed the observations from SEM. The long rod-like grains with micron sized features could only be observed for the samples fabricated at 300°C (**Figures S4-S5**). Kelvin-probe force microscopy (KPFM) mapping was performed to study the surface potential of Sb_2S_3 sulfurized at different temperatures. It is evident from **Figure S6** that all three samples have a very similar work function distribution at the surface, though the samples prepared at 300°C show an additional shoulder, indicating that some crystal faces have a different work function in these samples.

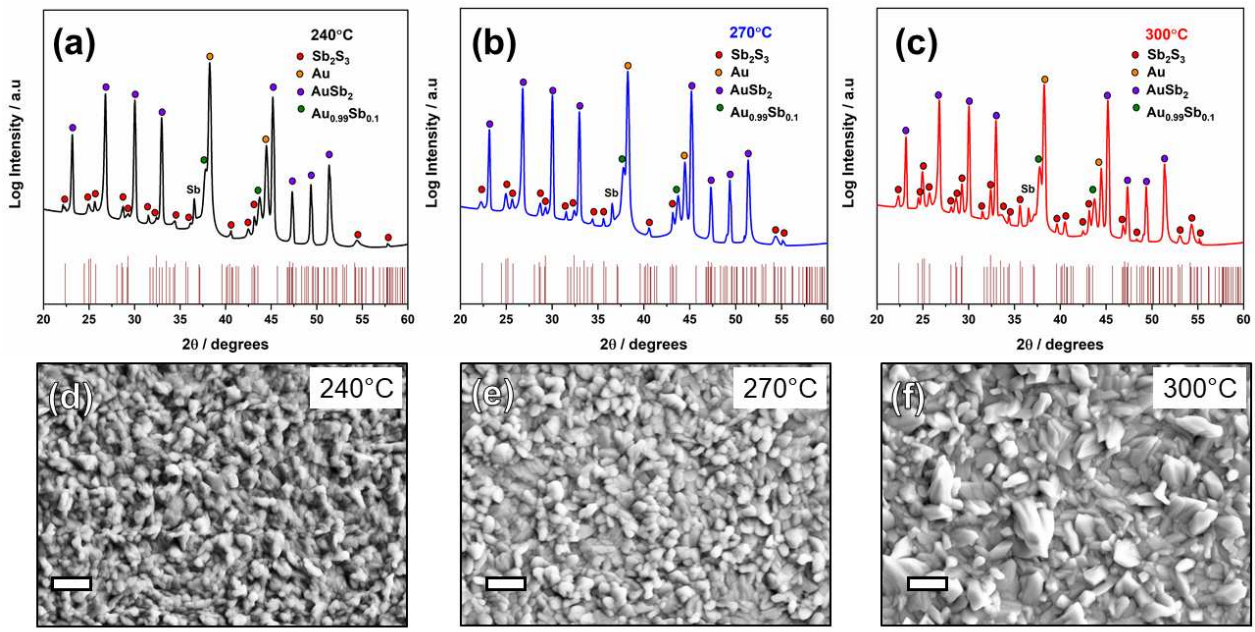

Figure 1. XRD of Sb_2S_3 thin films sulfurized at **(a)** 240°C, **(b)** 270°C, and **(c)** 300°C. SEM plan view for Sb_2S_3 synthesized by sulfurization at **(d)** 240°C, (**e)** 270°C, and **(f)** 300°C (scale bars are 600 nm).

Photoelectrochemical performance of Sb_2S_3 photocathodes

The as-prepared Sb_2S_3 thin films were coated with platinum (Pt) in order to evaluate their PEC performance for water splitting. The current density-voltage curves were obtained under 1 sun illumination in pH 0 (1 M H_2SO_4) in a 3-electrode configuration with a Pt wire as the counter electrode and Ag/AgCl as the reference electrode. **Figure 2 (a)** shows the PEC performance of such a photocathode with a maximum photocurrent density of ~ 0.7 mA cm^{-2}. Sb_2S_3 was found not to be stable in 1 M H_2SO_4 (pH 0) as evidenced from the inset of **Figure 2 (a)** where the photocurrent density rapidly decreased within 30 s. This lack of stability indicates that the Sb_2S_3 thin film requires coating with corrosion protection layers such as TiO_2, which has also been used as an electron collector in Sb_2S_3 sensitized solar cells.[15] Therefore, TiO_2 could act as both an electron collector and protection layer for the Sb_2S_3 photocathode.

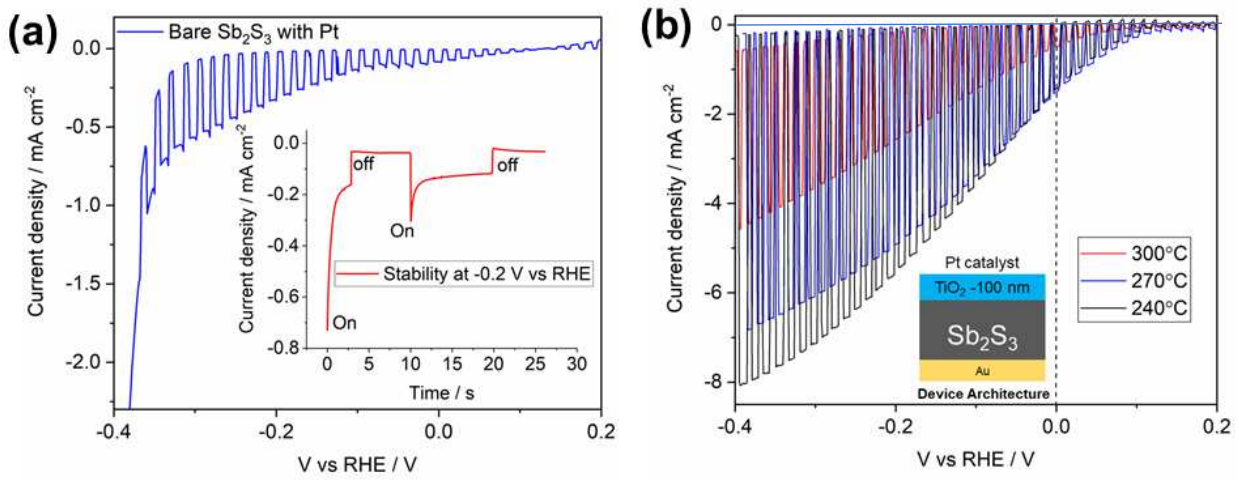

Figure 2. (a) Current density vs voltage plots for bare Sb_2S_3 coated with Pt catalyst in 1 M H_2SO_4 (pH 0) under 1 sun illumination. The inset shows the stability plot for Sb_2S_3/Pt photocathode under the same conditions. **(b)** Current density vs voltage plots for Au/Sb_2S_3/TiO_2 (100 nm)/Pt catalyst in 1 M H_2SO_4 (pH 0) under 1 sun illumination, with different sulfurization temperatures (inset shows the device architecture).

Atomic layer deposition (ALD) TiO_2 (100 nm) was deposited on the Sb_2S_3 thin films, followed by photo-electrodeposition of Pt to fabricate an ALD TiO_2-protected Sb_2S_3 photocathode. **Figure 2 (b)** shows the PEC performance of the different protected photocathodes synthesized at different sulfurization conditions (sulfurization temperature was varied and the sulfurization time was fixed at 40 mins as it yielded the best PEC performance (**Figure S7**)). It is evident that the 300°C sulfurized Sb_2S_3 has a later onset potential, a higher dark current and a lower photocurrent density than the 270°C and 240°C sulfurized Sb_2S_3. At more negative bias (-0.4 V vs RHE), photocurrent densities of around 8 mA cm^{-2} were obtained for the 240 °C sulfurized Sb_2S_3 photocathode. However, the photovoltage obtained was low (~0.1 V, as estimated from the onset potential). The protected Sb_2S_3 photocathodes exhibited a stable hydrogen evolution under 1 sun

illumination in 1 M H_2SO_4 for 12 hours (**Figure S8**), and the reproducibility of the devices was confirmed (**Figure S9**).

Band alignment studies of Sb_2S_3/TiO_2 junction by XPS

One possible reason for the low photovoltage in this system could be due to a large conduction band offset at the Sb_2S_3/TiO_2 heterointerface.[16] To assess the band offset between Sb_2S_3 and TiO_2, an XPS interface experiment was carried out. The band alignment was determined from the photoemission spectra, following a commonly practiced procedure as described in the literature.[17,18] The valence band maximum (VBM) and core level (CL) binding energies (BE) for Sb_2S_3 and TiO_2 were determined through measurements on thick layers of each material. XPS measurements of Sb_2S_3 show an energetic distance of the fermi level E_F to the valence band maximum E_{VBM} of ~1 eV, indicating that it is nearly intrinsic and even weakly n-type as the band gap of Sb_2S_3 is 1.7 eV (**Figure S10**). XPS measurements were then carried out versus increasing TiO_2 film thickness (0, 5, 10, 20, 50, 100 and 500 Å), allowing the Sb_2S_3 and TiO_2 VBMs at intermediate TiO_2 coverages to be tracked via shifts of the Sb $3d_{5/2}$, Sb 4d, S 2p, Ti $2p_{3/2}$ and S 2s core level binding energies. The BEs for the CL spectra were determined by fitting Voigt profiles (GL30) after performing a Shirley background subtraction. The position of the VBM was determined by a linear extrapolation of the low BE edge of the valence band emission.

For the determination of the band alignment, the peak positions of the substrate (Sb_2S_3) as well as the film (TiO_2) specific photoemission lines need to be considered. For intermediate coverage, the contributions from either TiO_2 or Sb_2S_3 are hard to distinguish in the VB spectra. However, by tracking the evolution of the CL BE with film thickness instead, the valence band offset for intermediate coverage can be extracted. The evolution of the CL BEs for all discussed interface experiments is given in **Figure 3 (a)** as a function of TiO_2 film thickness. For the Sb and

S CL BEs, a constant offset is applied to bring them to the same level as the VBM of the bare Sb_2S_3 substrate. A similar approach is used for the Ti and O CL BEs, which are referenced to the VBM of the thickest TiO_2 layer (50 nm). In this way, a change in the CL BE directly corresponds to a change in the VBM for the respective material if no interface reactions are observed. Such reactions would typically result in a non-uniform shift of the CL BE for a given material, which is not the case in the present study. ΔE_{VB} is calculated using the BE difference of the Sb $3d_{5/2}$ and Ti $2p_{3/2}$ peaks at intermediate coverage (ΔBE) as well as the BE of the Sb $3d_{5/2}$ ($BE_{Sb3d5/2\text{-}VBM}$) and Ti $2p_{3/2}$ ($BE_{Ti2p3/2\text{-}VBM}$) CLs with respect to the VBM:

$$\Delta E_{VB} = BE_{Sb3d5/2\text{-}VBM} - BE_{Ti2p3/2\text{-}VBM} - \Delta BE. \qquad (1)$$

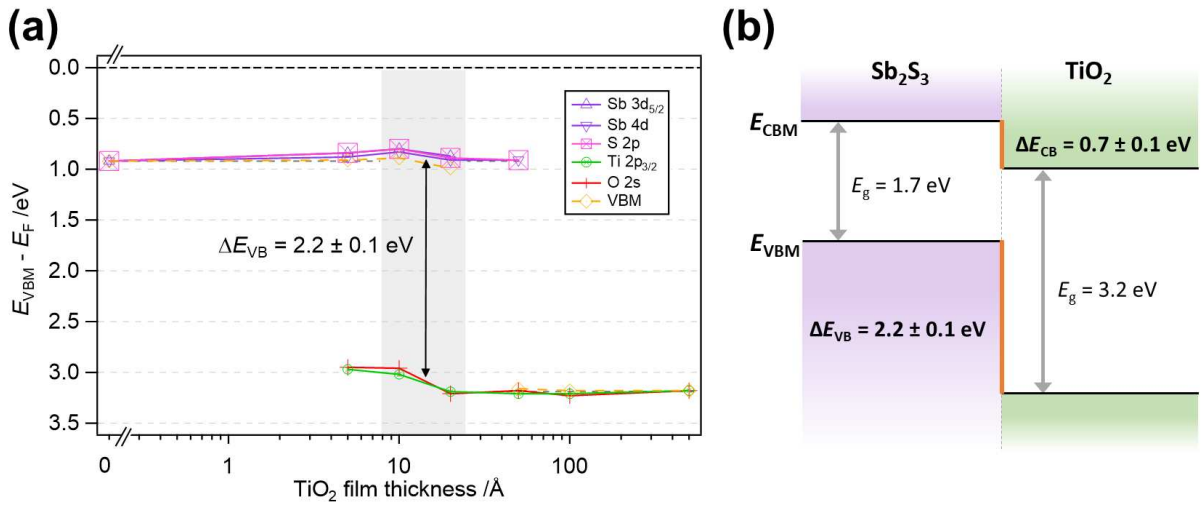

Figure 3. (a) XPS measurements of the valence band (VB) region for Sb_2S_3/TiO_2 with different thickness of TiO_2. **(b)** Experimentally determined band alignment of Sb_2S_3/TiO_2.

The valence band offset is found to be on the order of ΔE_{VB} = 2.2 eV ± 0.1 eV (**Figure 3(a)**). Using ΔE_{VB} and band gaps from the literature ($E_{g,Sb2S3}$ = 1.7 eV and $E_{g,TiO2}$ =3.2 eV) the conduction band offset, $\Delta E_{CB,}$ is determined according to:

$$\Delta E_{CB} = E_{g,Sb2S3} + \Delta E_{VB} - E_{g,TiO2}. \quad (2)$$

The corresponding offset is $\Delta E_{CB} = 0.7$ eV ± 0.1 eV and such a large conduction band offset could be one of the reasons for the low photovoltage observed in the Sb_2S_3 photocathodes (**Figure 3 (b)**).

Champion device PEC performance and bias dependent IPCE spectrum

The best performing (champion) device for 240 °C sulfurized Sb_2S_3 photocathode is shown in **Figure 4 (a)**, where photocurrent densities of ~ 9 mA cm^{-2} were obtained at -0.4 V vs RHE. The incident photon to current efficiency (IPCE) spectrum was obtained at 0 V vs RHE (**Figure 4 (b)**), and the integrated photocurrent density across the AM 1.5 G solar spectrum (3.4 mA cm^{-2}) matches well with the photocurrent density obtained from the current density-voltage curve measurements with our solar simulator (3.3 mA cm^{-2}). The onset of the IPCE spectrum was around 740 nm (1.7 eV), which matches the band gap of Sb_2S_3 (1.7 eV).[19]

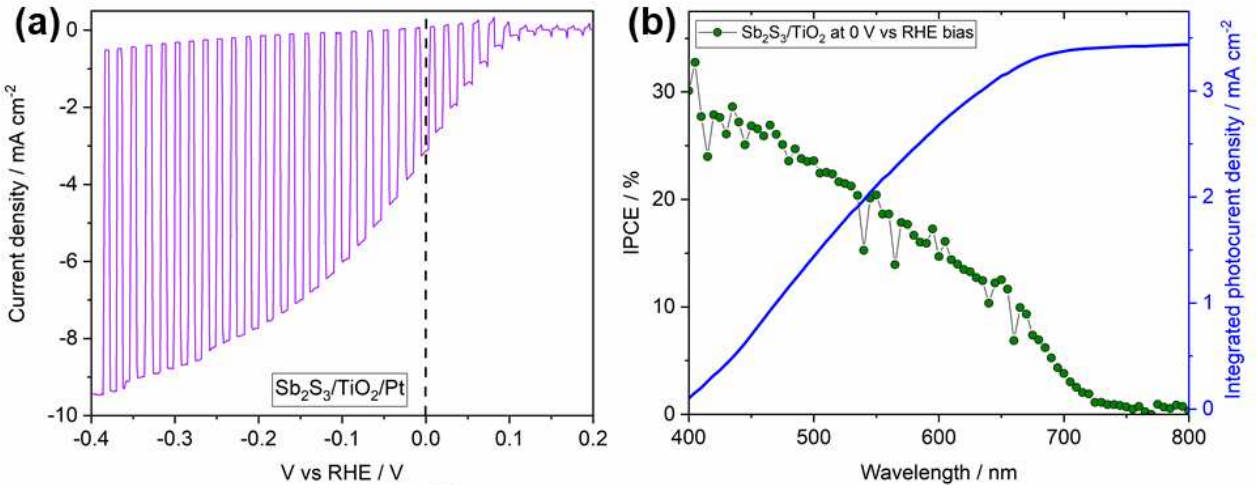

Figure 4. (a) Current density vs voltage plots for Sb_2S_3/TiO_2 (100 nm)/Pt catalyst in 1 M H_2SO_4 (pH 0) under 1 sun illumination (champion device, sample sulfurized at 240°C). (**b)** IPCE spectrum for Sb_2S_3/TiO_2/Pt photocathode under 0 V vs RHE bias in 1 M H_2SO_4 (pH 0) for the champion

device (Sb_2S_3 240°C sulfurized), and the integrated photocurrent density for the AM 1.5 G solar spectrum.

In order to gain further understanding of the wavelength dependent charge collection of our photocathodes, bias-dependent IPCE measurements were performed on the champion Sb_2S_3 sample (sulfurized at 240°C) (**Figure 5 (a)**). At positive bias (+0.05 V vs RHE), the IPCE near the band gap energy is low, increasing slowly with decreasing wavelength (from 740 nm to 400 nm). At an applied potential of 0 vs RHE an increase over the whole wavelength range by a factor of 2.2 can be observed in the IPCE (see also **Figure S11**). At -0.1 V vs RHE, however, a significant increase in the charge collection of blue photons (~400 nm) is evident. This observation can be explained by considering the initial band bending at the heterojunction and the wavelength-dependent penetration depth of the photons. Generally, the low energy photons are absorbed near the back contact of the absorbing film while the higher energy photons are absorbed closer to the heterojunction interface. From the band alignment (**Figure 3(b)**) and the Fermi level position of the ALD TiO_2,[20] an unfavorable band bending is predicted after equilibration of the Fermi levels (**Figure S12**), which arises due to the near intrinsic, weakly n-type Fermi level position of the Sb_2S_3. Due to the weak doping, the width of the space charge layer is large and extends deep into the film. Nearly no band bending is expected in the TiO_2 layer, as the films grown by ALD are highly doped (10^{20} cm^{-3}).[20] XPS results also confirm the high doping concentration as evidenced by the high fermi level position of TiO_2 (**Figure S10**). The barrier for electrons at the heterojunction interface can be overcome with a small bias (-0.1 V vs RHE, considering that the TiO_2 Fermi level is pinned to the electrolyte at ~0 V vs RHE) (**Figure S12**). The initial unfavorable band bending would trap photogenerated holes that are produced close to the Sb_2S_3/TiO_2 interface (generated from high energy photons) and lead to an increased recombination before collection. In contrast, the inversion of the unfavorable band bending by the small applied negative bias would drive the

photogenerated holes from the heterointerface to the back contact (**Figure S12**). This phenomenon can explain the larger impact of the applied bias for the blue photons.

Upon comparing the IPCE spectra of the samples prepared at 240°C and 300°C (**Figure 5 (b))** the explanation of the observed potential dependence of the blue photons for the 240°C sample can be further assessed. As shown by the AFM and SEM images, long rod like grains protrude from the surface for the 300°C sample (**Figure S3-S5**), which increases the path length for the photogenerated charge carriers to be collected, especially for shorter wavelengths that are generated near the photoabsorber surface. The onset of the IPCE at wavelengths 680-740 nm (which penetrate deep into the bulk of the semiconductor and enable the collection of photogenerated charge carriers near the back contact) is similar for both sulfurization temperatures. For shorter wavelengths though, the photon to current conversion efficiency decreases for the 300°C sample (**Figure 5(b)**). This observation (in combination with the AFM and SEM showing much longer rods for this sample type) is consistent with a charge carrier collection problem of photogenerated holes generated in the vicinity of the semiconductor/ electrolyte junction. Due to the larger grain size of the 300°C sample, the charge carriers will have to diffuse a longer distance to reach the back contact of the films in order to separated. This would result in higher charge carrier recombination and hence yielding lower PEC performance for the 300°C sample.

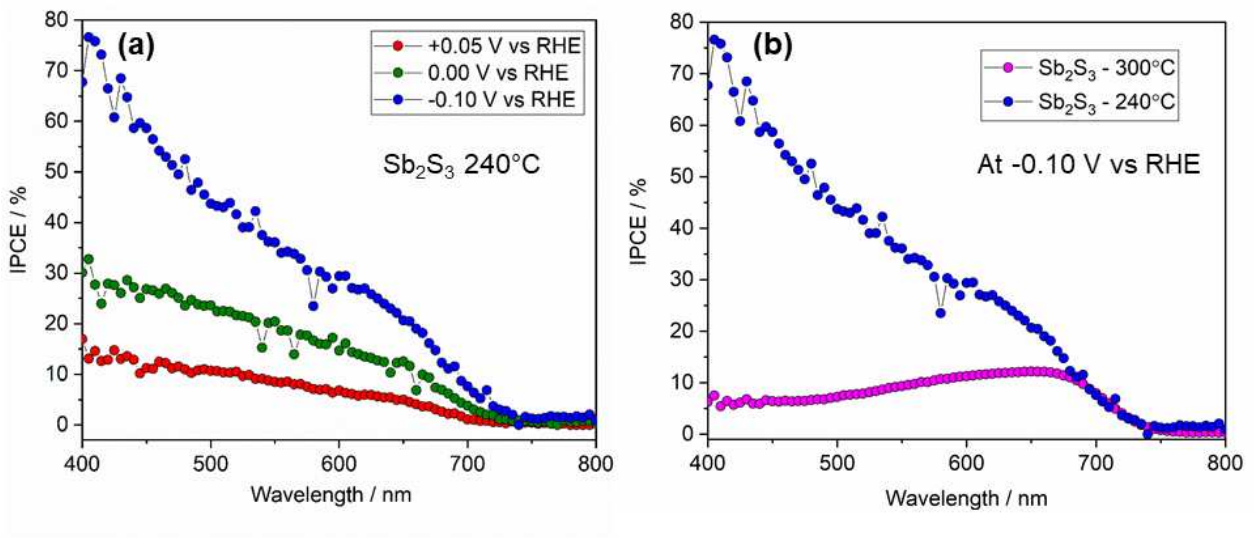

Figure 5. (a) IPCE spectrum for the $Sb_2S_3/TiO_2/Pt$ champion device from Figure 4 (a) under different bias vs RHE in 1 M H_2SO_4 (pH 0). **(b)** IPCE spectrum for $Sb_2S_3/TiO_2/Pt$ photocathodes (240°C and 300°C) under -0.10 V vs RHE in 1 M H_2SO_4 (pH 0).

It is worth noting that, despite having an unfavorable band bending at the heterojunction interface (**Figure S12**), the Sb_2S_3 photocathodes does inject significant photoelectrons into the TiO_2 layer for water reduction. The observations also imply that upon a controlled p-type doping of the absorber (for instance with Cu) a higher built in voltage in the heterojunction can be generated. The more favorable band bending would likely result in an increased V_{oc}, and an increase in the collection efficiency of the charge carriers would also improve the photocurrent. Further, the presence of $AuSb_2$ at the back contact could be detrimental to the PEC performance as the work function may be unfavorable. Gold has been reported to be an ohmic contact for Sb_2S_3 in solar cells and having only gold at the back contact could potentially yield higher PEC performance.[21]

Sb_2S_3/In_2S_3 junction for improved photovoltage

Another approach to increase the PEC performance of our photocathodes is to implement a more

suitable buffer layer than TiO_2. The introduction of a buffer layer with better conduction band alignments with Sb_2S_3 junction (i.e. low conduction band offset) could result in reduced interfacial recombination and would therefore improve the photovoltage generated from the junction.[22,23] In_2S_3 has been reported to have a conduction band position of 0.3-0.4 eV higher than TiO_2 and hence could yield potentially a higher photovoltage.[24,25] Therefore, $Sb_2S_3/In_2S_3/TiO_2/Pt$ photocathodes were fabricated in order to test whether larger photovoltage could be achieved. In_2S_3 was deposited by chemical bath deposition on the Sb_2S_3 (270°C) thin films followed by TiO_2 (100 nm) and Pt as a hydrogen evolution catalyst. **Figure 6** shows the current density plots for the $Sb_2S_3/In_2S_3/TiO_2$ /Pt photocathode. An earlier onset potential was observed (~ 0.25 V vs RHE), showing an improvement of 0.15 V when compared to the $Sb_2S_3/TiO_2/Pt$ photocathode. However, the lower slope of the rise in the photocurrent density with respect to voltage indicates an increased series resistance (**Figure 6 and Figure S13**). The increased series resistance could be due to an upward band bending in the In_2S_3/TiO_2 interface if the fermi level position of In_2S_3 is energetically higher than that of the TiO_2 fermi level. Nevertheless, the increase in onset potential could be due to an improved band alignment in these samples.

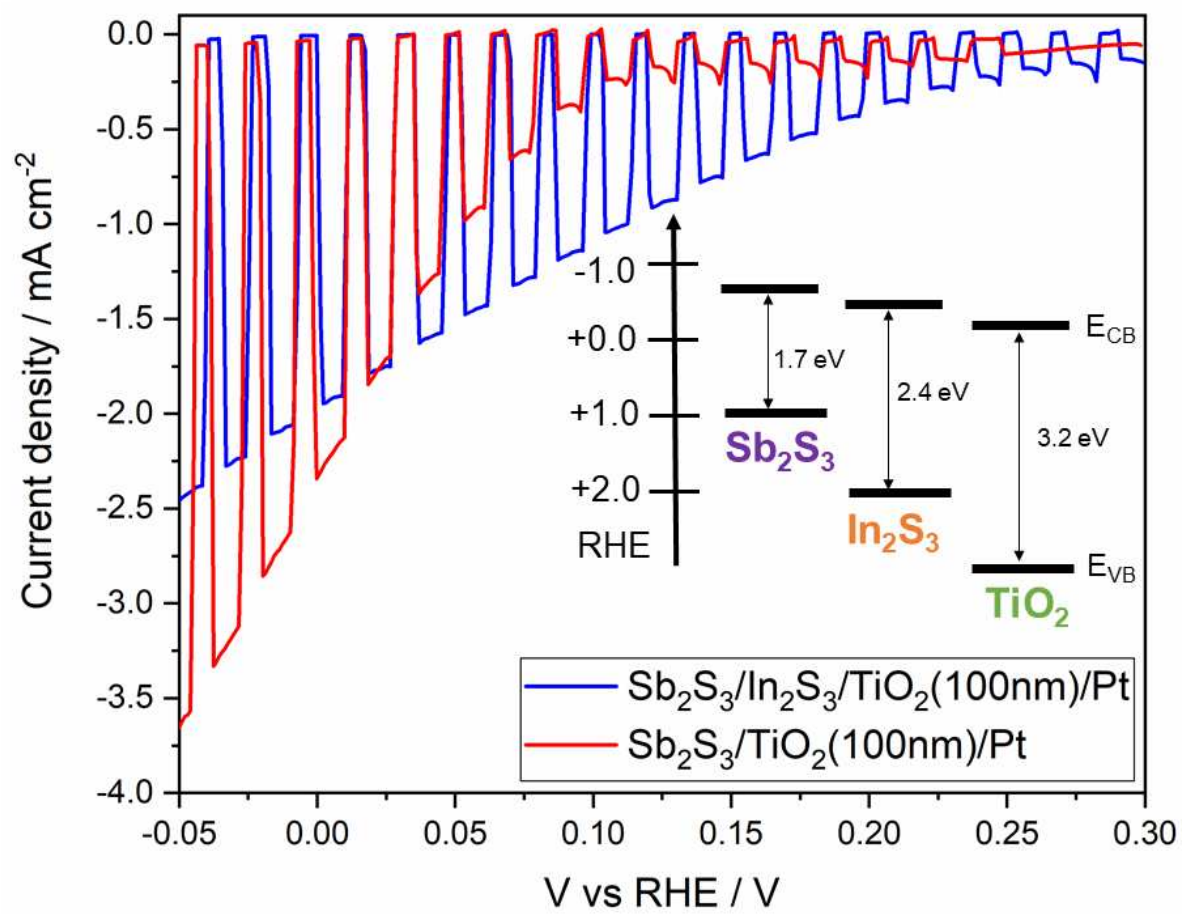

Figure 6. Current density vs voltage plots for Sb_2S_3(270 °C)/In_2S_3/TiO_2/Pt photocathode and Sb_2S_3(270 °C)/TiO_2/Pt photocathode in 1 M H_2SO_4 (1 sun illumination).

CONCLUSION

We synthesized Sb_2S_3 by a simple sulfurization of Sb metal prepared by electrodeposition at relatively low temperatures and demonstrated the use of a TiO_2 buffer/protection layer for water splitting applications, yielding photocurrent densities of 3 mA cm^{-2} at 0 V vs RHE and ~ 9 mA cm^{-2} at more negative bias. However, the photovoltage as estimated from the onset potential was low (~ 0.1 V). From XPS band alignment studies and bias dependent IPCE measurements, the low photovoltage was attributed to the near intrinsic, weakly n-type nature of Sb_2S_3 (weak band bending

at the Sb_2S_3/TiO_2 junction), short diffusion length (poor collection of charge carriers generated in the bulk evidenced by IPCE) and the large conduction band offset of Sb_2S_3/TiO_2 junction. The photovoltage was improved by employing a buffer layer (In_2S_3) with a higher lying conduction band position, thus reducing the conduction band offset and giving an earlier onset potential (~ 0.25 V photovoltage). This work also demonstrates that In_2S_3 is a promising junction material for Sb_2S_3. Further improvements in controlling the doping (making p-type Sb_2S_3 for downward conduction band bending at the junction) and band alignment of Sb_2S_3 (buffer layers with conduction band position nearer to that of Sb_2S_3) will make it increasingly attractive for cost-effective large-scale water splitting.

ASSOCIATED CONTENT

Supporting information

The supporting information is available free of charge via the Internet at http://pubs.acs.org.

Synthesis schematic, XRD, AFM height images, KPFM images, device long term stability measurements, device reproducibility, XPS, normalized IPCE spectra and proposed band bending schemes.

AUTHOR INFORMATION

Corresponding Author

S. David Tilley – *Department of Chemistry, University of Zurich, Winterthurerstrasse 190, CH-8057 Zurich, Switzerland;* Email: david.tilley@chem.uzh.ch

Authors

Rajiv Ramanujam Prabhakar - *Department of Chemistry, University of Zurich, Winterthurerstrasse 190, CH-8057 Zurich, Switzerland;*

Thomas Moehl - *Department of Chemistry, University of Zurich, Winterthurerstrasse 190, CH-8057 Zurich, Switzerland;*

Sebastian Siol - *Empa Swiss Federal Laboratories for Materials Science and Technology, Überlandstrasse 129, CH-8600 Dübendorf, Switzerland*

Jihye Suh - *Department of Chemistry, University of Zurich, Winterthurerstrasse 190, CH-8057 Zurich, Switzerland;*

Author Contributions

The manuscript was written through contributions of all authors. All authors have given approval to the final version of the manuscript.

ACKNOWLEDGEMENTS

This work was supported by the University of Zurich, the University Research Priority Program (URPP) LightChEC, and the Swiss National Science Foundation (AP Energy Grant # PYAPP2 160586).

REFERENCES

(1) Kondrotas, R.; Chen, C.; Tang, J. Sb2S3 Solar Cells. *Joule* **2018**, *2* (5), 857–878.

(2) Ghosh, C.; Varma, B. P. Optical Properties of Amorphous and Crystalline Sb2S3 Thin Films. *Thin Solid Films* **1979**, *60* (1), 61–65.

(3) Choi, Y. C.; Lee, D. U.; Noh, J. H.; Kim, E. K.; Seok, S. Il. Highly Improved Sb2S3 Sensitized-Inorganic–Organic Heterojunction Solar Cells and Quantification of Traps by Deep-Level Transient Spectroscopy. *Adv. Funct. Mater.* **2014**, *24* (23), 3587–3592.

(4) Yuan, S.; Deng, H.; Dong, D.; Yang, X.; Qiao, K.; Hu, C.; Song, H.; Song, H.; He, Z.; Tang, J. Efficient Planar Antimony Sulfide Thin Film Photovoltaics with Large Grain and Preferential Growth. *Sol. Energy Mater. Sol. Cells* **2016**, *157*, 887–893.

(5) Savadogo, O.; Mandal, K. C. Low Cost Schottky Barrier Solar Cells Fabricated on CdSe

and Sb2 S 3 Films Chemically Deposited with Silicotungstic Acid. *J. Electrochem. Soc.* **1994**, *141* (10), 2871–2877.

(6) Zhang, J.; Liu, Z.; Liu, Z. Novel WO3/Sb2S3 Heterojunction Photocatalyst Based on WO3 of Different Morphologies for Enhanced Efficiency in Photoelectrochemical Water Splitting. *ACS Appl. Mater. Interfaces* **2016**, *8* (15), 9684–9691.

(7) Song, Y.-T.; Lin, L.-Y.; Chen, Y.-S.; Chen, H.-Q.; Ni, Z.-D.; Tu, C.-C.; Yang, S.-S. Novel TiO2/Sb2S3 Heterojunction with Whole Visible-Light Response for Photoelectrochemical Water Splitting Reactions. *RSC Adv.* **2016**, *6* (54), 49130–49137.

(8) DeAngelis, A. D.; Kemp, K. C.; Gaillard, N.; Kim, K. S. Antimony(III) Sulfide Thin Films as a Photoanode Material in Photocatalytic Water Splitting. *ACS Appl. Mater. Interfaces* **2016**, *8* (13), 8445–8451.

(9) Wang, Y.-C.; Zeng, Y.-Y.; Li, L.-H.; Qin, C.; Wang, Y.-W.; Lou, Z.-R.; Liu, F.-Y.; Ye, Z.-Z.; Zhu, L.-P. A Stable and Efficient Photocathode Using an Sb2S3 Absorber in a Near-Neutral Electrolyte for Water Splitting. *ACS Appl. Energy Mater.* **2020**. https://doi.org/https://doi.org/10.1021/acsaem.0c00210.

(10) Prabhakar, R. R.; Septina, W.; Siol, S.; Moehl, T.; Wick-Joliat, R.; Tilley, S. D. Photocorrosion-Resistant Sb2Se3 Photocathodes with Earth Abundant MoSx Hydrogen Evolution Catalyst. *J. Mater. Chem. A* **2017**, *5* (44), 23139–23145.

(11) Gunawan; Septina, W.; Harada, T.; Nose, Y.; Ikeda, S. Investigation of the Electric Structures of Heterointerfaces in Pt- and In2S3-Modified CuInS2 Photocathodes Used for Sunlight-Induced Hydrogen Evolution. *ACS Appl. Mater. Interfaces* **2015**, *7* (29), 16086–16092.

(12) Waldrop, J. R.; Grant, R. W.; Kowalczyk, S. P.; Kraut, E. A. Measurement of Semiconductor Heterojunction Band Discontinuities by X-ray Photoemission Spectroscopy. *J. Vac. Sci. Technol. A* **1985**, *3* (3), 835–841.

(13) Siol, S.; Hellmann, J. C.; Tilley, S. D.; Graetzel, M.; Morasch, J.; Deuermeier, J.; Jaegermann, W.; Klein, A. Band Alignment Engineering at Cu2O/ZnO Heterointerfaces. *ACS Appl. Mater. Interfaces* **2016**, *8* (33), 21824–21831.

(14) Parize, R.; Cossuet, T.; Chaix-Pluchery, O.; Roussel, H.; Appert, E.; Consonni, V. In Situ Analysis of the Crystallization Process of Sb2S3 Thin Films by Raman Scattering and X-Ray Diffraction. *Mater. Des.* **2017**, *121*, 1–10.

(15) Wang, X.; Li, J.; Liu, W.; Yang, S.; Zhu, C.; Chen, T. A Fast Chemical Approach towards

Sb2S3 Film with a Large Grain Size for High-Performance Planar Heterojunction Solar Cells. *Nanoscale* **2017**, *9* (10), 3386–3390.

(16) Brandt, R. E.; Young, M.; Park, H. H.; Dameron, A.; Chua, D.; Lee, Y. S.; Teeter, G.; Gordon, R. G.; Buonassisi, T. Band Offsets of N-Type Electron-Selective Contacts on Cuprous Oxide (Cu2O) for Photovoltaics. *Appl. Phys. Lett.* **2014**, *105* (26), 263901.

(17) Siol, S.; Schulz, P.; Young, M.; Borup, K. A.; Teeter, G.; Zakutayev, A. Combinatorial In Situ Photoelectron Spectroscopy Investigation of Sb2Se3/ZnS Heterointerfaces. *Adv. Mater. Interfaces* **2016**, *3* (24), 1600755.

(18) Klein, A. Energy Band Alignment at Interfaces of Semiconducting Oxides: A Review of Experimental Determination Using Photoelectron Spectroscopy and Comparison with Theoretical Predictions by the Electron Affinity Rule, Charge Neutrality Levels, and the Common Anion. *Thin Solid Films* **2012**, *520* (10), 3721–3728.

(19) Medina-Montes, M. I.; Montiel-González, Z.; Paraguay-Delgado, F.; Mathews, N. R.; Mathew, X. Structural, Morphological and Spectroscopic Ellipsometry Studies on Sputter Deposited Sb2S3 Thin Films. *J. Mater. Sci. Mater. Electron.* **2016**, *27* (9), 9710–9719.

(20) Moehl, T.; Suh, J.; Sévery, L.; Wick-Joliat, R.; Tilley, S. D. Investigation of (Leaky) ALD TiO2 Protection Layers for Water-Splitting Photoelectrodes. *ACS Appl. Mater. Interfaces* **2017**, *9* (50), 43614–43622.

(21) Deng, H.; Zeng, Y.; Ishaq, M.; Yuan, S.; Zhang, H.; Yang, X.; Hou, M.; Farooq, U.; Huang, J.; Sun, K.; et al. Quasiepitaxy Strategy for Efficient Full-Inorganic Sb2S3 Solar Cells. *Adv. Funct. Mater.* **2019**, *29* (31), 1901720.

(22) Li, C.; Hisatomi, T.; Watanabe, O.; Nakabayashi, M.; Shibata, N.; Domen, K.; Delaunay, J.-J. Positive Onset Potential and Stability of Cu2O-Based Photocathodes in Water Splitting by Atomic Layer Deposition of a Ga2O3 Buffer Layer. *Energy Environ. Sci.* **2015**, *8* (5), 1493–1500.

(23) Lee, Y. S.; Chua, D.; Brandt, R. E.; Siah, S. C.; Li, J. V; Mailoa, J. P.; Lee, S. W.; Gordon, R. G.; Buonassisi, T. Atomic Layer Deposited Gallium Oxide Buffer Layer Enables 1.2 V Open-Circuit Voltage in Cuprous Oxide Solar Cells. *Adv. Mater.* **2014**, *26* (27), 4704–4710.

(24) Liu, X.; Zheng, H.; Zhang, J.; Xiao, Y.; Wang, Z. Photoelectric Properties and Charge Dynamics for a Set of Solid State Solar Cells with Cu4Bi4S9 as the Absorber Layer. *J. Mater. Chem. A* **2013**, *1* (36), 10703–10712.

(25) Li, Y.; Luo, S.; Wei, Z.; Meng, D.; Ding, M.; Liu, C. Electrodeposition Technique-

Dependent Photoelectrochemical and Photocatalytic Properties of an In2S3/TiO2 Nanotube Array. *Phys. Chem. Chem. Phys.* **2014**, *16* (9), 4361–4368.